J. Fluid Mech. (1966), *vol.* 25, *part* 2, *pp.* 377–400
Printed in Great Britain

The constraints imposed on tornado-like vortices by the top and bottom boundary conditions

By J. S. TURNER

Woods Hole Oceanographic Institution, Woods Hole, Massachusetts†

(Received 28 June 1965 and in revised form 1 December 1965)

A laboratory model of a tornado vortex has been produced, incorporating two features which are believed to be important to the understanding of the atmospheric phenomenon, but which have been largely ignored in previous studies. First, it has been shown that a vortex can be driven from *above* by a mechanism analogous to convection in a cloud, and that density differences within the funnel itself are not essential. Associated with this mechanism of formation is a circulation in the vertical, with an upflow in the centre surrounded by a compensating annular downflow. Secondly, the bottom boundary is seen to have a strong influence on the vortex, since the down and up flows are linked there by a rapid radial inflow in a thin boundary layer.

In the present paper an approximate theoretical description of such a vortex is proposed. The interior and boundary layer flows are first examined separately, and then a condition is sought which makes the two solutions consistent. The starting-point of the theory is the assumption of a form of stream function which describes a circulation in the vertical having the essential features of that observed. The result of the matching procedure is to fix both the form of the tangential velocity profile, and the relative magnitudes of the three components of velocity. These deductions are not critically dependent on the assumed form of the motion in the vertical, and are in good agreement with the first measurements in the laboratory vortices, though the quantitative experimental results are not emphasized here.

1. Introduction

In view of the longstanding interest in tornadoes, surprisingly little is known about their detailed characteristics, either from observation or theory. There is, for example, no general agreement about even the direction of vertical motion in the funnel. Much of the difficulty of observation can probably be attributed to the fact that tornado vortices are usually made visible by markers which are not good indicators of air motions: the descending edge of the cloud funnel outlines a pressure surface rather than indicating downward air motions, and trajectories of heavy debris do not trace particle paths either. Theories too are divided, on the question of the relative importance of driving by buoyancy within the funnel, or by a pressure gradient imposed from above.

† Present address: Department of Applied Mathematics and Theoretical Physics, Silver St., Cambridge.

Associated with the theoretical approaches to the problem have been many laboratory investigations, in some of which extremely realistic-looking vortices have been produced. The ease with which such phenomena can be exhibited, however, has probably actually retarded development in the field. As Fultz (1951) pointed out in his review of the subject, these 'experiments lead only to conclusions that result also from elementary theory and go back to the seventeenth and eighteenth century beginnings of the discussion'. They all provide some means of producing angular momentum and of concentrating this by an inflow towards the centre of rotation, but few investigators have attempted any quantitative measurements, or have even compared the nature of the boundary conditions imposed on their flows with those appropriate for tornadoes. There therefore still seems to be a great need for quantitative studies of experimental vortices. The useful models will not necessarily be those which resemble the atmospheric case in every respect; but more attention should be paid to comparisons between the experiments and nature to discover if the laboratory results are relevant at all.

In a previous paper (Turner & Lilly 1963), we took a first step in this direction, and suggested a new method of producing tornado-like vortices in the laboratory. These are driven by a mechanism which we believe is closely analogous to convection in the atmosphere. A stream of gas bubbles released at the centre of the top of a rotating tank causes an upflow and consequently a circulation in the vertical, and the radial inflow associated with this concentrates the pre-existing angular momentum in a central core. The bubbles driving the motion may either be released by nucleation of carbonated water, or injected directly through a fine tube. We suggested two advantages that this method might have over the common one of withdrawing fluid from the container (as described, for example, by Long 1958). First, a steady state can be obtained without the need to return fluid to the container at an arbitrarily chosen radius, usually the outer rim, and secondly, the vertical motion near the region of convection is free to adjust itself to the vortex motion which it produces, a condition which must be satisfied in the atmosphere.

In the case where bubbles are injected into the tank from a compressed air line, the flow can be kept steady indefinitely, and the various velocity profiles measured by photographing the motion of small marker particles. Much can be deduced about the flow in advance of detailed quantitative measurements, however, by observing the behaviour of dye. The first important observation is that a vortex can be driven over the whole depth of the tank by the region of convection at the top. The motion in the centre is upwards, and surrounding this region of upflow is an annulus in which there is a downflow (see plate 1, figure 1). After a long time, dye injected into the flow fills the whole of a central cylindrical region and does not appear outside it (plate 2, figure 2), showing that the radial and vertical velocities fall off rapidly with radial distance. The increased angular velocities are also confined to this region.

The relevance of this picture of the cylindrical confinement of a vortex driven from above has received support recently from some observations of waterspouts made by Thorarinsson & Vonnegut (1964) in unusual circumstances.

They photographed a series of spouts formed under the smoke plume rising from an active volcano near Iceland. Outside the condensation funnels there is often visible a much wider cylinder filled with ash which has clearly been pulled down from above. We suggest that this might be more generally the case, but that only rarely is there a suitable tracer of air motion such as the fine ash present on this occasion.

Further deductions can be made about our laboratory flow by following the motion of dye in more detail. Dye injected at the top of the tank moves downwards with its tip at nearly constant radius through the whole depth (plate 1, figure 1), but the velocity decreases from top to bottom. The vertical velocity does not appear to decrease towards zero at the bottom however. As the dye approaches the bottom, it suddenly reappears closer to the centre and moves upwards, indicating that a rapid inward radial transport is taking place in a thin boundary layer (see figure 6). The vertical velocity profile must be such that the central upward and the annular downward transports are exactly equal at any height, and the radial flow in the boundary layer must be closely matched to the vertical flow. In this experiment the flow both into and out of the boundary layer is smooth and non-turbulent.

It is clear from these observations that the boundaries at both the top and bottom of the vortex can have a profound influence on the flow. It is the aim of this paper to examine the theory of such flows with the boundary conditions on the axis particularly in mind, and to show that a relation between the vertical and circulating motions must exist, as a consequence of the constraints imposed by the lower boundary. Certain special problems of this kind have recently been solved numerically by those interested in vortex tubes. Workers in that field have very clearly recognized the importance of boundary-layer effects, and we shall later use some of the results of their investigations. Many of these have unfortunately only appeared in laboratory reports with limited circulation, but a convenient summary of this work is to be found in a report of a recent symposium on concentrated vortex motions in fluids (Küchemann 1965).

The main arguments of the present work can be outlined very simply. Starting with a stream function which is suggested by, and has all the essential properties of, the laboratory vortex described above, the tangential velocity profile can be calculated in two ways. First, a set of 'interior solutions' is obtained from the form of the radial inflow, using the equations appropriate to strong vortices in a region away from solid boundaries. This is essentially the method which has been used in the past for the sink vortex, and it leads to a set of profiles corresponding to different strengths of the inflow. The same form of stream function also implies a certain distribution of the inward flux in the boundary layer, as a function of radius. Since this flux is produced by an unbalanced pressure gradient associated with the tangential motion, a second set of tangential profiles can be deduced for various strengths of the axial flow. The requirement that the profiles found in these two ways should have the same position and magnitude of the velocity maximum fixes not only the form of the tangential profile, but also the magnitude of all the velocities.

2. Vortices with strong circulation

First, let us consider the steady axisymmetric flow of a viscous incompressible fluid in a region remote from solid boundaries. The most relevant work on this subject is that of Lewellen (1962). He has developed a series expansion method for studying such flows when the circulation is strong, which justifies earlier approximate calculations and shows how their accuracy can be assessed and higher order terms found. A summary of his results will now be given, in a form which will be applicable to our case.

A stream function $\hat{\psi}$ for the vertical motion is introduced, such that

$$u = \frac{1}{r}\frac{\partial \hat{\psi}}{\partial z}, \quad w = -\frac{1}{r}\frac{\partial \hat{\psi}}{\partial r}. \tag{1}$$

By eliminating the pressure, the equations of motion and continuity for axisymmetric motion can be reduced to two, in the dependent variables $\hat{\psi}$ and $\hat{\Gamma} = vr$, the circulation. A further simplification is obtained by using dimensionless variables, defined for the present purpose in the form

$$\eta = \left(\frac{r}{r_0}\right)^2, \quad \xi = \frac{z}{l}, \quad \Gamma = \frac{\hat{\Gamma}}{\Omega r_0^2}, \quad \psi = \frac{\hat{\psi}}{u_0 r_0 l}, \tag{2}$$

where r_0, l, Ω and u_0 are appropriate scales of horizontal and vertical length, angular velocity and radial velocity, the meaning of which will be made more explicit later. The resulting regrouping shows that the flow is in general governed by three parameters

$$\left.\begin{aligned} N &= \frac{u_0 r_0}{\nu} && \text{the radial Reynolds number,} \\ \alpha_0 &= \left(\frac{r_0}{l}\right)^2 && \text{the square of the ratio of characteristic lengths,} \\ \text{and} \quad \epsilon &= \left(\frac{u_0 l}{\Omega r_0^2}\right)^2 && \text{the square of the ratio of typical vertical and tangential velocities.} \end{aligned}\right\} \tag{3}$$

Lewellen first examined the special case, considered earlier by Rott (1958) and by Donaldson & Sullivan (1960), for which

$$\Gamma = \Gamma(\eta), \quad \psi = \xi f(\eta). \tag{4}$$

He showed that this form results in the elimination of both α_0 and ϵ, and that solutions of this type cannot satisfy axial boundary conditions in which there is a radial variation of the axial pressure gradient. They cannot therefore be exact solutions either for the sink flow or the 'tornado' type we are considering here. Lewellen's major contribution was his description of a method which can in principle take into account *any* variation of this axial pressure gradient. By making a series expansion of Γ and ψ in the parameter ϵ (which is small in many flows of interest, including our laboratory experiment and tornadoes in the atmosphere), he showed that the zeroth-order equations are

$$\Gamma_0 \frac{\partial \Gamma_0}{\partial \xi} = 0 \quad \text{or} \quad \Gamma_0 = \Gamma_0(\eta), \tag{5}$$

and
$$2\eta\frac{\partial^2\Gamma_0}{\partial\eta^2}-N\frac{\partial\Gamma_0}{\partial\eta}\frac{\partial\psi_0}{\partial\xi}=0. \tag{6}$$

The most general form of ψ_0 consistent with (6) is

$$\psi_0=f_{00}(\eta)+\xi f_{01}(\eta), \tag{7}$$

and therefore
$$2\eta\Gamma_0''-Nf_{01}\Gamma_0'=0, \tag{8}$$

where primes denote differentiation with respect to η.

To this order of approximation then the radial and tangential velocities are independent of height and the vertical velocity at any radius changes linearly with height. So far, no boundary conditions have been specified, but the functions f_{00} and f_{01} must be chosen with these in mind. Any f_{01}, or distribution of inflow velocity, which is consistent with the boundary conditions may be specified, and then Γ_0 found by integrating (8). This result is the justification of the method used, for example, by Einstein & Li (1951) in their calculation of tangential velocity profiles in the sink vortex. They assumed in effect a certain distribution of inflow, and then calculated the circulation profile for various values of N. The systematic procedure devised by Lewellen allows one to calculate also the higher-order correction terms, and assess the accuracy of the zeroth-order approximation.

Reference should also be made to Lewellen's discussion of two other well-known theoretical studies of vortices which have had the tornado in mind, but which differ in important respects from the present approach. Long (1958, 1961) found similarity solutions valid in a core boundary layer near the axis. These imply, however, that the axial and tangential velocities are of the same order everywhere, and they are therefore not appropriate when ϵ is small. Gutman (1957), on the other hand, found similarity solutions for a special case of a vortex driven along its length by buoyancy produced by the release of latent heat. Such effects might certainly be relevant sometimes in the atmosphere, but in the following we will be guided by the laboratory experiment and consider a fluid of constant density on which a vertical motion is imposed from above.

3. The application of the strong circulation equation to our laboratory vortices

Lewellen applied his method to the case of flow in a vortex tube, with tangential injection and axial withdrawal of fluid. In order to do this, he again had to assume a special form of stream function which seemed appropriate to the flow through the hole. Experimentally, however, the situation was much more complex, since the end walls of the chamber imposed different boundary conditions on the flow to the ones assumed, and led to a 'secondary flow' which in fact closely resembles the vertical circulation observed in our experiments. More recently, this boundary-layer interaction problem has been studied in greater detail by Rosenzweig, Lewellen & Ross (1964), and by Rott & Lewellen (1965).

The lack of agreement between Lewellen's original calculation and the observations does not imply any weakness in his method, however. It just means that

the stream function chosen did not represent all the required features of the flow. If a stream function more appropriate to the vertical circulation actually observed can be written down, then the procedure can again be used to find the corresponding tangential velocity profile. The experimental conditions for our convectively driven vortex seem more clear-cut than they are in the usual vortex tube arrangements, and we will regard what we observe as the *primary* flow. In this section we discuss more appropriate forms of stream function to describe this vertical motion and then apply Lewellen's method to calculate the tangential profiles.

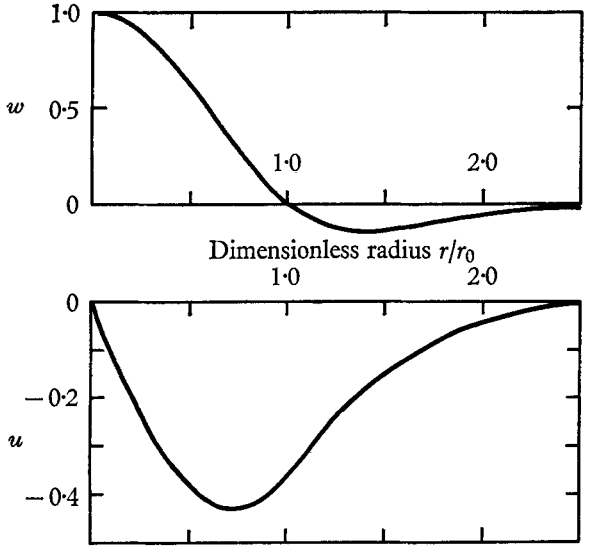

FIGURE 3. The forms of the vertical (w) and radial (u) velocity profiles given by equations (10) in the text. The profiles calculated from (11) are very similar, except that u falls to zero at $r/r_0 = \beta^{-\frac{1}{2}}$.

The simplest form of non-dimensional stream function which, (*a*) satisfies the condition (7) imposed by strong circulation or small ϵ, (*b*) represents an upflow at $r = 0$ and a surrounding downflow, and (*c*) becomes small at large radii, is

$$\psi = -\eta e^{-\eta}(1+\xi). \tag{9}$$

The corresponding vertical and radial velocities are

$$w = 2u_0 \frac{l}{r_0}(1-\eta)\, e^{-\eta}(1+\xi), \quad u = -u_0 \eta^{\frac{1}{2}} e^{-\eta}. \tag{10}$$

These forms are drawn as a function of $r/r_0 = \eta^{\frac{1}{2}}$ in figure 3. Explicit meanings can now be given to r_0 and u_0: r_0 is the radius at which the vertical velocity vanishes, and u_0 is e times the radial velocity at that radius. The first calculations were made using these functions, but it later seemed slightly preferable to generalize (9) to a form which allows ψ to become zero at a finite radius, namely,

$$\psi = -\eta(1-\beta\eta)\, e^{-\alpha\eta}(1+\xi). \tag{11}$$

The parameter β is determined by the radius of zero ψ, and α may be related to it if we again take the position of zero w as our horizontal length scale r_0. In this

case $\alpha = (1-2\beta)/(1-\beta)$ and (11) is a family of profiles specified by the single parameter β.

Notice that in taking the forms (9) and (11) we have gone beyond what is implied by the assumption of strong circulation alone. We have also put

$$f_{00} = f_{01} = -\eta(1-\beta\eta)\, e^{-\alpha\eta}, \tag{12}$$

which is not required by (7). It implies that the vertical velocity profiles are similar at all heights, and that the radial mass flux in the bottom boundary layer has the same functional form as the flux per unit height in the interior. With this assumption the definition of the vertical length scale does not depend on radius; l is the depth over which the total radial inflow equals that in the boundary layer, or equivalently, the height at which the stream function doubles from its

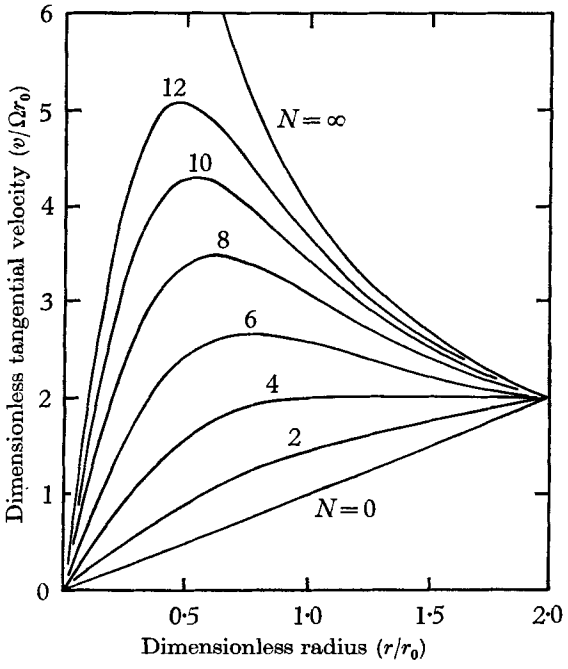

FIGURE 4. 'Interior' profiles of tangential velocity, calculated using equation (13) with $\beta = \frac{1}{4}$, $\alpha = \frac{2}{3}$ and a series of values of N.

value at the outer edge of the bottom boundary layer. It is not strictly necessary at this point to assume this relation between f_{00} and f_{01}, but a connexion between them is needed when the boundary-layer matching procedure is carried out later. Near the axis $\eta = 0$, the assumption $f_{00} = f_{01} \to \eta$ is certainly required by the boundary conditions. The assumed forms are also in accord with what we observe, and in particular with the cylindrical form of the region of upward motion and the fact that the zero of vertical velocity is at the same radius everywhere. How accurately (12) can be satisfied at larger radii will be discussed again in a later section. A detailed theoretical justification of this procedure must await a study of the upper boundary condition, which is not considered in this paper apart from the vertical velocity distribution it produces.

With f_{01} of the form given by (11) the equation (8) for Γ_0 becomes

$$\Gamma_0'' + \tfrac{1}{2}N(1-\beta\eta)e^{-\alpha\eta}\Gamma_0' = 0. \tag{13}$$

If we suppose that the angular velocity scale Ω is just the angular velocity of the tank, all the non-dimensional quantities are now fully specified. Equation (13) allows us to calculate sets of profiles of Γ_0 or v as a function of η or r/r_0, for different values of N and β. There are now only two boundary conditions at our disposal; the most important constraint is clearly $\Gamma_0(0) = 0$. For convenience of integration the slope at the origin was also specified, but the resulting solutions were afterwards scaled to give $\Gamma_0 = \eta$ at $\eta = 1/\beta$, i.e. so that the tangential velocity reached solid rotation at the radius where the radial velocity is zero.

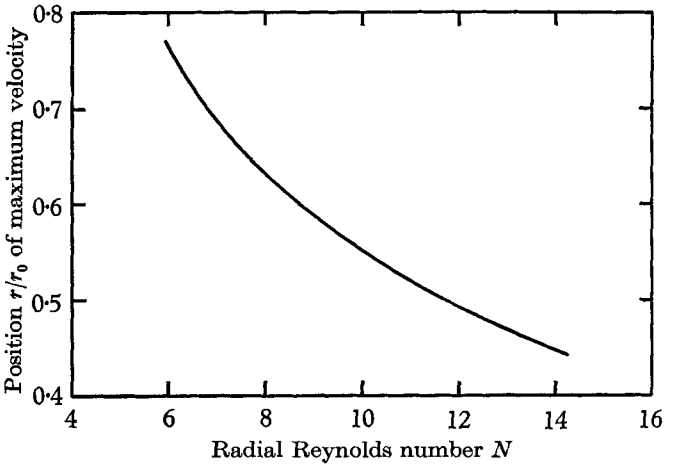

FIGURE 5. The position of the maximum tangential velocity for profiles like those in figure 4, as a function of N. Within the range of β used ($\frac{1}{6}$ to $\frac{1}{4}$), the curves for different β are indistinguishable from one another on the scale used here.

In figure 4 are shown the results of integrating (13) numerically for a series of values of N with $\beta = \frac{1}{4}$ (and therefore $\alpha = \frac{2}{3}$). Similar results have been obtained with other values of β, corresponding to different ratios of the radii of regions of upflow and downflow. The form (11) is preferred to (9) because it suggests a definite reason for fixing on an outer radius at which to apply the second boundary condition on (13). Equation (9) was at first used in much the same way, but only by specifying arbitrarily (but with an eye on the experimental results) the radius at which solid rotation was approached. The part of these profiles at even larger radii is not very useful, since the zeroth-order approximation is poor there; more terms are necessary to produce a solution approaching a given solid rotation at large radii, which it is not possible for the zeroth-order term to do alone.†

The main features of these tangential profiles, which will be significant later, are the strong dependence of both the maximum velocity and the radius at which this occurs on N. (In figure 5, for example, the radial position of the maximum

† I am indebted to Mr Albert Barcilon for his investigation of this point.

has been plotted against N.) For $N = 0$, or very large viscosity, the fluid is everywhere in solid rotation. As N increases, a maximum in v develops at an intermediate radius. Near the axis is a viscous core which is nearly in solid rotation, and whose angular velocity increases with increasing N. Similar features are of course observed in the solutions of Einstein & Li (1951), who worked with different assumed radial velocities. The solution of Rott (1958) also exhibits the same kind of viscous core.

4. The boundary-layer theories

Various methods of approach to the problem of a rotating fluid over a solid boundary have been developed. Von Kármán (1921) first considered the related problem of the flow in a stationary fluid due to a rotating disk. Bödewadt (1940) solved numerically the equations for the flow produced over an infinite stationary plane in a fluid which is rotating with uniform angular velocity at infinite distance from the plane. Batchelor (1951) discussed qualitatively the general class of flows of which these two are the limiting examples. More recently Rogers & Lance (1960) have studied numerically similarity solutions for the case where the plane and the fluid are rotating with arbitrary angular velocities. A number of workers, notably Mack (1962) and Rott & Lewellen (1964), have used a momentum integral approach, and have applied their methods to special types of non-uniform outer flow. Most of these theories have an application to vortex tubes in mind, but Lewellen (in an unpublished thesis, and in the report just quoted) has commented on the possible importance of boundary interaction effects for the tornado vortex.

Though the momentum integral methods offer the best hope for a full quantitative solution of the problem, the work which seems most readily applicable in the present context is that of Rogers & Lance (1960). We will first summarize their results, and then suggest a plausible extension of them to the case of non-uniform rotation of the outer flow. The results obtained in this way are consistent with what is observed in our model, but their quantitative use does involve an extra assumption which is not investigated in detail here.

When the outer flow is rotating with angular velocity ω, greater than that of the boundary Ω, Rogers & Lance introduce non-dimensional variables defined by

$$\left.\begin{aligned} \Omega = \sigma\omega, \quad \zeta = z(\omega/\nu)^{\frac{1}{2}}, \\ u = r\omega F(\zeta), \quad v = r\omega G(\zeta), \quad w = (\nu\omega)^{\frac{1}{2}} H(\zeta). \end{aligned}\right\} \tag{14}$$

The radial and transverse velocity profiles F and G have been calculated as functions of ζ for various σ. These have an oscillatory character, with alternate layers of fluid moving inward and outward along the disk. The net volume flux per unit circumference is *inwards*, of magnitude

$$M = \int_0^\infty u\,dz = r(\nu\omega)^{\frac{1}{2}} \int_0^\infty F(\zeta)\,d\zeta. \tag{15}$$

Using the profiles of F presented by Rogers & Lance for various σ, we can proceed a step further than they did, and write down an explicit expression for

the dependence of M on σ. In the range $0 \leqslant \sigma < 1$ it is numerically very closely true that

$$\int_0^\infty F(\zeta)\, d\zeta = 0{\cdot}67(1-\sigma), \tag{16}$$

so that the radial volume flux per unit length is

$$M = -0{\cdot}67(1-\sigma)\, r(\nu\omega)^{\frac{1}{2}}, \tag{17}$$

inserting the negative sign appropriate to inward transport.

5. The extension to a non-uniform outer flow

All the results of the previous section are strictly for an outer flow in solid rotation. We will now make a local similarity assumption, and suppose that the inward flux in the boundary layer at any radius is related to the *local* angular velocity ω by the same expression (17) obtained using the above similarity transformations. We can see immediately that (17) has the sort of behaviour which is required in our application: the radial flux vanishes at the axis and where the angular velocity of the interior flow equals that of the bottom, and has a naximum in between. These features are characteristic also of solutions obtained by the momentum integral method for all cases in which the circulation decreases with decreasing radius. Again the assumption is likely to be most accurate near the axis, where the tangential flow approaches solid rotation. A non-uniform radial flux in the boundary layer of course implies a non-uniform vertical velocity at large distances above the boundary, and the type of behaviour suggested by our laboratory experiment is sketched in figure 6. Note that the results of Rogers & Lance will be used here in the opposite way to that commonly employed in studies of boundary layers under rotating flows: that is, the vertical velocity profile will be assumed given, and the corresponding tangential profiles deduced.

Continuity of mass implies that the vertical velocity at the edge of the bottom boundary layer is related to the change of radial flux in the boundary layer by

$$w(r, 0) = -\frac{1}{r}\frac{\partial(rM)}{\partial r}. \tag{18}$$

Comparing with (1) we see that

$$\hat{\psi}_{\xi=0} = rM, \tag{19}$$

if $\hat{\psi}$ is zero at $r = 0$. Inserting now the form (7) appropriate to strong circulation and using (17) gives

$$u_0 \frac{l}{r_0} f_{00} = -0{\cdot}67(1-\sigma)\, \eta(\nu\omega)^{\frac{1}{2}}. \tag{20}$$

With the special form (11) for f_{00} (20) becomes

$$C(1-\beta\eta)\, e^{-\alpha\eta} = (1-\sigma)\, \sigma^{-\frac{1}{2}}, \tag{21}$$

where

$$C = 1{\cdot}50\, (\Omega\nu)^{-\frac{1}{2}} u_0 \frac{l}{r_0}; \tag{22}$$

or, expressing this parameter in terms of ϵ, α_0 and N defined in (3),

$$C = 1{\cdot}50 N^{\frac{1}{2}} \alpha_0^{-\frac{1}{2}} \epsilon^{\frac{1}{2}}. \tag{22a}$$

Equation (21) can be solved explicitly for σ as a function of η to give the angular velocity profile in the interior corresponding to a given form of vertical motion. A family of solutions is obtained for various values of the parameter C, whose magnitude is proportional to the ratio of characteristic vertical and boundary-layer velocities. Some of these solutions, for the profiles with $\beta = \frac{1}{4}$, are shown in figure 7. Notice that the magnitude of the maximum velocity is sensitive to C, but the radius at which this occurs changes much less than it does for the 'interior' profiles of figure 4. In fact for the form of vertical velocity used here, this position moves slowly inward to the limit $r/r_0 = 0{\cdot}5$ (whatever the value of β) as C or the central angular velocity becomes large. The behaviour of the maximum is shown in figure 8 for several values of β.

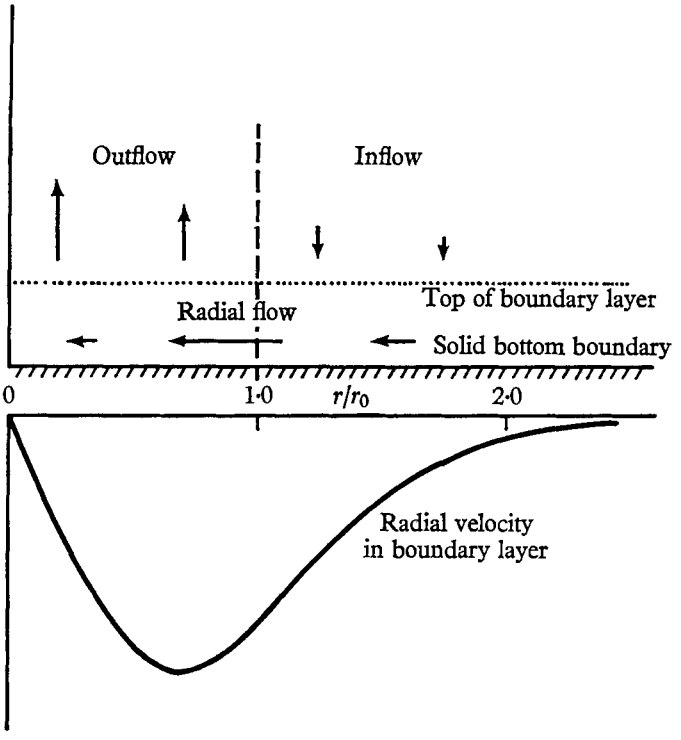

FIGURE 6. A sketch of the bottom boundary layer, illustrating how the radial inflow in this layer must be related to the vertical flow outside it.

It is worth noting at this point that there is an upper limit to the value of C for which tangential profiles obtained in this way could be realized physically. The steep region of negative slope near $r = r_0$ implies that the angular momentum is increasing slowly with increasing radius. As a certain value of C is exceeded, this rate of increase becomes zero at some radius, and then negative. Such profiles would be unstable to small disturbances, so that already the lower boundary has apparently imposed a limit on the magnitude of tangential velocity which can co-exist with the form of vertical motion chosen. For the 'matched' profiles described in the next section, this occurs first with $C = 4{\cdot}4$ when $\beta = 0{\cdot}234$, and the corresponding maximum tangential velocity is $3{\cdot}9\,\Omega r_0$.

This result is not in fact very helpful, since it probably only exhibits the increasing inadequacy of our assumptions, about the form of vertical profile and local similarity, at larger radii. The vertical motion in a steady vortex driven by convection must always adjust itself in such a way that the angular momentum *does* increase outwards.

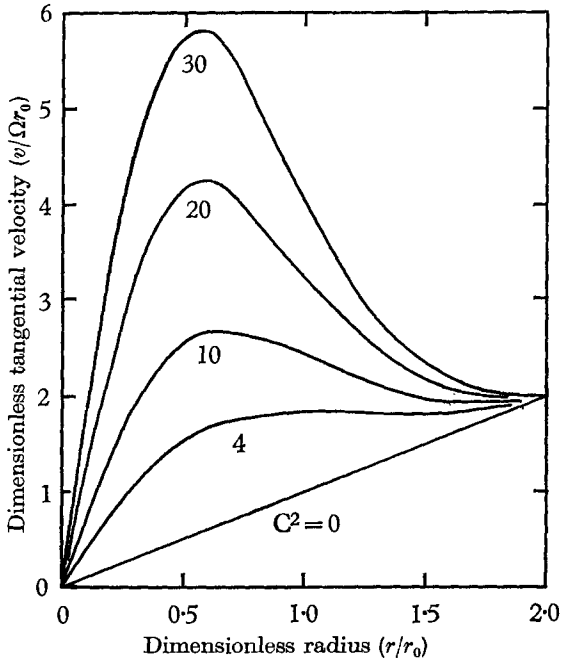

FIGURE 7. Profiles of tangential velocity, calculated using a local similarity assumption to relate radial flow in the boundary layer to the local angular velocity. These are solutions of equation (21), with $\beta = \frac{1}{4}$, $\alpha = \frac{2}{3}$ and various values of C.

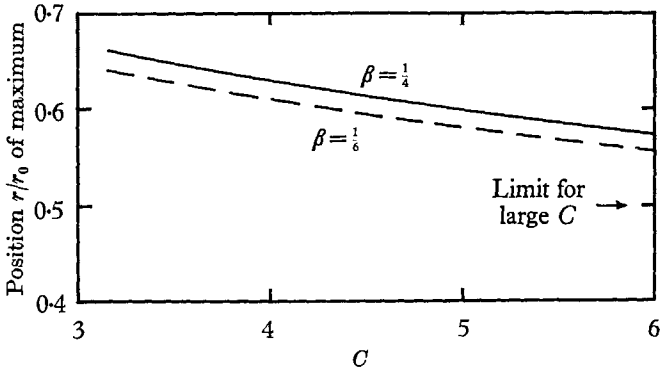

FIGURE 8. The position of the maximum tangential velocity for profiles like those in figure 7, as a function of C. The curves are displaced slightly for different β, but all tend to $r/r_0 = 0{\cdot}5$ for large C.

6. Comparison of the interior and boundary-layer solutions

We now come to the most important step of the argument: the demonstration that the possible range of conditions, for which the 'interior' and 'boundary-layer' solutions of §§ 3 and 5 are valid simultaneously, is small. It will be shown that this requirement fixes the values of both N and C within certain limits.

For each assumed form of the stream function in the vertical (corresponding to a given β, or a given ratio of the radii of the upflow and the downflow) two sets of tangential profiles have been obtained, as shown in figures 4 and 7. It is now necessary to pick out a pair, one from each set, which are as similar as possible in shape. These should have at least the same position and magnitude of the velocity maximum, and if possible have the same slope at the origin. (The choice of the vertical stream function has already ensured that they reach solid rotation at the same radius.) In figures 9 and 10 are plotted the magnitude of the velocity maximum and the angular velocity at the origin against the position of the maximum for the two sets of solutions, for $\beta = \frac{1}{4}$ and $\beta = \frac{1}{6}$. As remarked earlier, the position of the maximum for the interior solutions is much more sensitive to changes in parameters than it is for the boundary-layer solutions. The curves for the two cases therefore cross, and this permits the determination of a unique set of parameters corresponding to each form of motion in the vertical. It happens that both the velocity maxima and the angular velocity at the origin match with very nearly the same position of the maximum.

With $\beta = \frac{1}{4}$ the values obtained are $(r/r_0)_{\max} = 0{\cdot}62$; $v_{\max} = 3{\cdot}6 r_0 \Omega$; $\omega_0 = 11\Omega$. From the previous figures 5 and 8 we see that the profiles picked out in this way fix the magnitudes of N and C too, and we find $N = 8{\cdot}2$, $C^2 = 18$ ($C = 4{\cdot}2$). The corresponding values with $\beta = \frac{1}{5}$ and $\beta = \frac{1}{6}$ and therefore wider regions of downflow are shown in table 1. Notice that the position of the maximum and the value of N are rather insensitive to β (or the position of the outer edge of the annular downflow), whereas C, the magnitude of the maximum, and especially the magnitude of the central angular velocity, are much more dependent on β. This small variation of N and $(r/r_0)_{\max}$ is of course a direct consequence of the small variations of $(r/r_0)_{\max}$ in the 'boundary-layer' curves on figures 9 and 10, and it remains true if we relax the condition $f_{00} = f_{01}$ and compare the boundary layer and interior curves for *different* β.

The 'matched' pairs of profiles for $\beta = \frac{1}{4}$ and $\beta = \frac{1}{6}$ are shown in figure 11. They are indistinguishable on this scale from the origin to the maximum, but the fit becomes worse at larger radii, especially for small values of β. The 'boundary-layer' solution, though it is poor in an intermediate range, preserves the correct asymptotic behaviour at large radii, whereas the 'interior' profiles go very wrong there. This reflects the fact that higher order terms in the ϵ expansion are small at small η, but must become large in order to produce a solution approaching a given solid rotation. It seems likely too that the exact form of the assumed stream function becomes more important in this region, and that the assumption $f_{00} = f_{01}$ can no longer be made if consistency between the two methods of calculating the tangential motion is to be obtained.

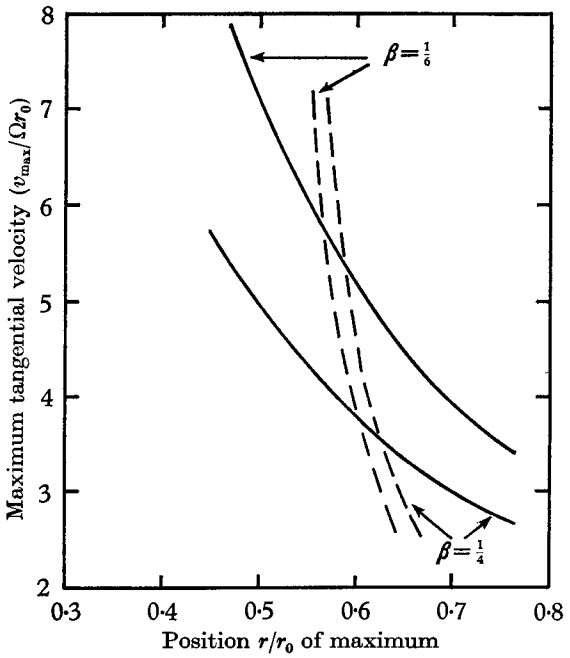

FIGURE 9. The magnitude of the maximum tangential velocity plotted against its position, using profiles like those in figures 4 and 7 with two values of β. Solid lines: 'Interior' profiles; broken lines: 'boundary-layer' calculation.

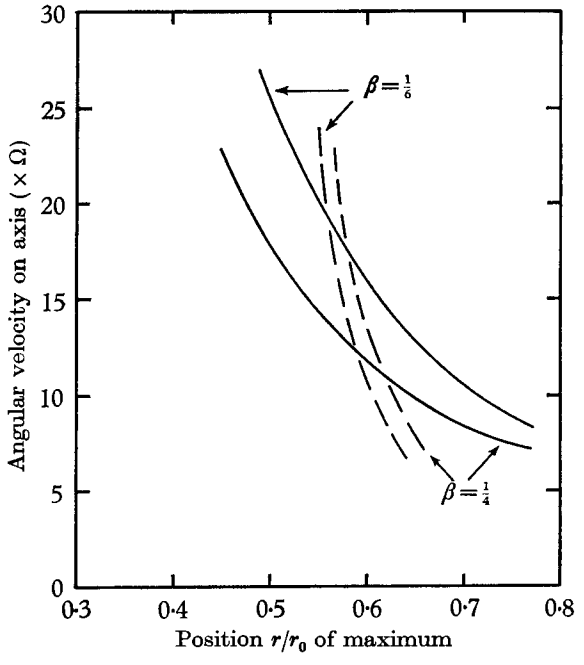

FIGURE 10. The angular velocity along the axis, plotted against the position of the maximum tangential velocity for the same profiles used in preparing figure 9.

β	(r/r_0) at max	$v_{max}/r_0\Omega$	$\omega_{r=0}/\Omega$	N	C
$\frac{1}{4}$	0·62	3·6	11	8·2	4·2
$\frac{1}{5}$	0·59	4·6	15	8·9	4·9
$\frac{1}{6}$	0·57	5·8	19	9·6	5·5

TABLE 1. The properties of the theoretical tangential velocity profiles obtained by comparing the interior and boundary-layer solutions

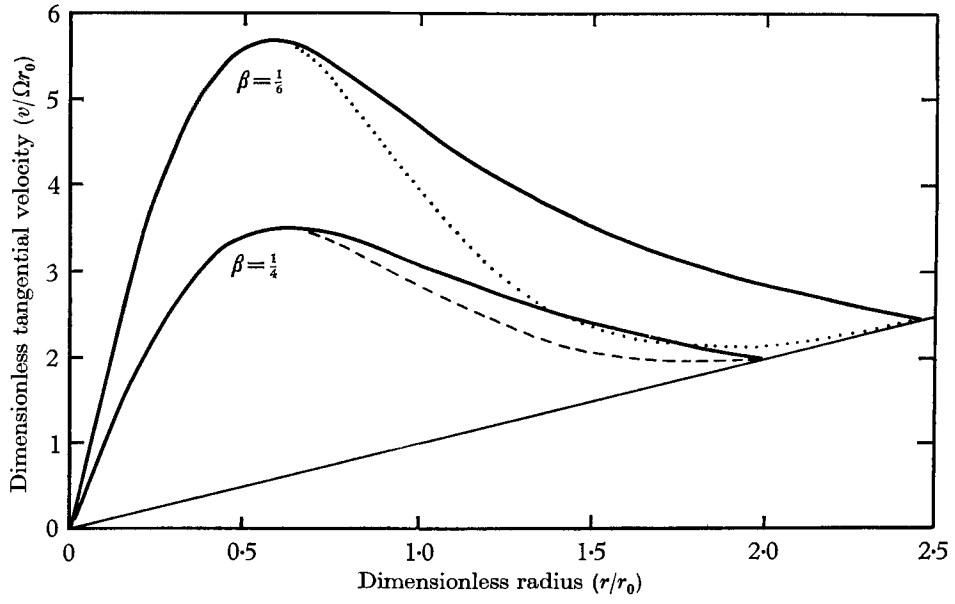

FIGURE 11. Matched pairs of tangential velocity profiles for two values of β. 'Interior' profiles (full lines) and 'boundary-layer' profiles (broken lines) have been chosen to have the same position and magnitude of the maximum, using figure 9. They also have the same angular velocity along the axis.

Let us now return to (22*a*), and examine what is implied by fixing the parameters N and C according to the matching condition. This imposes a relation between α_0 and ϵ of the form

$$\epsilon = b\alpha_0, \tag{23}$$

where b is a numerical factor of order unity. (Its value is $b = 0{\cdot}95$ when $\beta = \frac{1}{4}$ and $b = 1{\cdot}9$ when $\beta = \frac{1}{6}$.) There is thus now only one free parameter in the problem, which may be taken as either α_0 or ϵ. It is clear from (23) that a small ratio of horizontal to vertical length scales is sufficient to ensure the small value of ϵ which is required to justify the use of the zeroth-order approximation.

7. Solutions obtained without assuming a form of stream function

The above matching procedure has led to a satisfactory agreement between tangential profiles obtained in two ways, provided the form of the stream function for the vertical motion is assumed to be known. We now inquire if it is possible to eliminate the specific assumption about the vertical motion, and

determine this too from the boundary-layer matching. This can in fact be done, but for reasons which will become apparent, less definite information is obtained in this way than by using the preceding calculation.

By retaining the assumption $f_{00} = f_{01}$, but now without using the specific form (12), f_{00} can be eliminated from (8) and (20) to give an equation for Γ_0:

$$\Gamma_0'' + \frac{N}{2C}(1-\sigma)\sigma^{-\frac{1}{2}}\Gamma_0' = 0, \tag{24}$$

where $\Gamma_0 = \eta/\sigma$. This can be integrated numerically from $\Gamma_0 = 0$ at $\eta = 0$ and gives a family of solutions whose character depends on the parameter

$$N/2C = \frac{1}{3}\frac{r_0^2}{l}\left(\frac{\Omega}{\nu}\right)^{\frac{1}{2}},$$

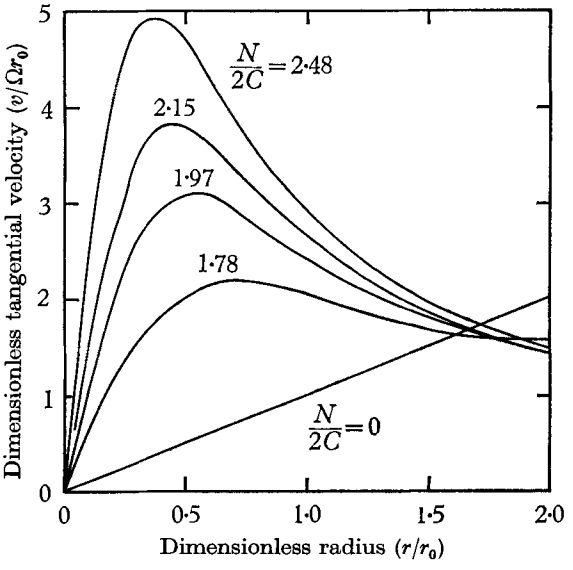

FIGURE 12. Profiles of tangential velocity calculated using the condition $f_{00} = f_{01}$ but with no explicit assumption about the form of f_{01}.

a combination of the horizontal and vertical length scales and the boundary-layer depth. So far, r_0 has not been specified and the slope of Γ_0 is arbitrary at the origin. In order to make the solutions directly comparable with those obtained earlier, r_0 has been defined as the position of zero w, or the maximum of $f_{00}(\eta)$ calculated from (24) and (20). The numerical solutions scaled in this way are shown in figure 12 as functions of $\eta^{\frac{1}{2}}$ and the corresponding values of $N/2C$ are marked on the curves. (These are irregularly spaced because Γ_0' at $\eta = 0$ has been fixed as an initial value for the integration, and $N/2C$ determined later by scaling Γ_0 and η by the same factor in (24).) The stream functions have not been plotted, but their form may be deduced from (20). They rise from zero at $\eta = 0$ to a maximum at $\eta = 1$, and fall to zero at $\sigma = 1$, where the angular velocity of the flow is the same as that of the bottom. This occurs at nearly the same value of $\eta^{\frac{1}{2}}$ for

all the profiles shown. It is clear that the vertical velocity will not be zero at that radius, though the radial velocity must be.

Qualitatively, therefore, these solutions do exhibit the behaviour which is necessary to represent the laboratory experiments, an angular velocity which decreases rapidly away from the centre, and a central upflow surrounded by an annular downflow. They have, however, retained many of the features of the 'interior' profiles found earlier. One has no control over the form of v or of f at large radii: both of these functions oscillate with large amplitude, the former about $v = r\Omega$ and the latter about $f = 0$. The position of the first maximum of v is sensitive to the value of $N/2C$ and is related to its magnitude in a similar way to that already shown in figure 9 for the interior profiles. The magnitude suggests an outer fitting point at a smaller radius, which is also consistent with figure 12.

The usefulness of this procedure is limited by the fact that there is now no clear way to choose *one* of these solutions, or to impose the observed behaviour on v or f at large radii. As has already been pointed out, it is not possible to assign a further boundary condition at large radii (and in particular to approach solid rotation there) using the zeroth-order approximation alone. The assumption $f_{00} = f_{01}$ on which the derivation of (24) is based is also likely to be inadmissible at larger radii (cf. figure 11). Only by including terms of higher order, or by using the full equations for the interior motion, can one expect to obtain solutions of the proper form at large radii. It seems possible that this outer boundary condition could then pick out a unique solution, as it did in the problem considered by Gutman (1957).

8. Summary of properties obtained by matching

The arguments developed in this paper have led to many explicit relations between measurable flow parameters, as a result first of the assumption of large swirl and then the matching conditions imposed at the bottom boundary. These results will be collected together, and in some cases rewritten in a more convenient form, before they are compared with the available experiments.

Fundamental to the whole argument is the assumption that ϵ is small, and this should be tested directly from the definition $\epsilon = (u_0 l/\Omega r_0^2)^2$. An immediate consequence of the 'large swirl' (small ϵ) condition is the linear variation of w with height: this too can be tested, and the values of $w(0, \xi)$ along the axis provide a measure of l/r_0, by the definition of l, and of u_0, using the relation obtainable from (11)

$$w(0, 0) = 2u_0 l/r_0. \tag{25}$$

The profile of vertical velocity should be compared with the assumed forms, and r_0 is of course defined as the radius of zero vertical velocity.

The prediction has been made that $N = u_0 r_0/\nu$ should have a narrow range of numerical values near $N = 9$. The quantities needed can again be obtained from the variation of w with height. If a direct measurement of radial velocity, say u_1 at $r = r_0$ can also be made, then N might be obtained alternatively using values of u_0 deduced from (11). (For example, $u_0 = 2{\cdot}60u_1$ when $\beta = \frac{1}{4}$.)

The addition of a known value of angular velocity to the parameters already available will now allow the calculation of C, from (22). As shown in table 1,

this can vary more widely than N and is sensitive to the value of β, i.e. to the relative radii of the regions of up- and downflow. Closely linked to the changes in C are the differences in the predicted tangential profiles which are also set out in table 1. A result which remains valid in spite of wide variations in the other quantities is that the position of the maximum should lie near $r/r_0 = 0{\cdot}60$.

Other results which are not tested extensively here, but which may be useful in future comparisons with experiment, are relations between the three components of velocity. These depend on the ratio of length scales r_0/l, which is left as a free parameter in the problem, provided only that it is small. They may be obtained from the data recorded in table 1 and written in the form

$$\frac{u_{\max}}{w(0,0)} = c_1 \frac{r_0}{l}, \quad \frac{w(0,0)}{v_{\max}} = c_2 \frac{r_0}{l}. \tag{26}$$

Again the results are not very sensitive to β: the factor c_1 is 0·22 for $\beta = \frac{1}{4}, \frac{1}{6}$; and $c_2 = 0{\cdot}54$ when $\beta = \frac{1}{4}$, $c_2 = 0{\cdot}48$ when $\beta = \frac{1}{6}$.

9. Preliminary comparison with experiment

Laboratory experiments were conducted concurrently with the development of the ideas set out above. The most important deductions from them have been qualitative, and it has been shown how these experiments suggested the method of approach used here. Some quantitative results are also available, however, and are worth recording, even though they were obtained before the behaviour was well understood, and not all the quantities later recognized to be important were measured in every case. Enough data are available to show at least that this theoretical approach is relevant to these experiments (and in particular to check that ϵ *is* small) and to provide a first test of the conclusions. The experiments to be described do not cover a wide range of conditions, partly because a fixed geometry was used throughout, but partly for a reason over which we had less control. The ability of the driving stream of bubbles to adjust itself to the vortex it produces is probably an important factor in achieving a match between the vertical and tangential motions, but there is an associated disadvantage: there is no convenient *external* parameter available to use for a comparison between experiments. The magnitude of the vertical motion produced by this bubbling must be used instead, and this is not related in a simple way to the rate of air flow.

Results are available for two different upper boundary conditions, a free surface and rigid lid (with a hole in the centre to allow the air to escape). The rigid lid made it possible to achieve a completely steady state for very much longer than with the free surface, probably because it supplies angular momentum to the vortex more effectively and eliminates waves on the surface which eventually move the vortex away from the centre. With a rigid lid, on the other hand, the oscillations of vertical velocity are large, and waves pass up the centre much as they would along a loose helical spring stretched from top to bottom of the tank.

The basic velocity measurements were made by injecting neutrally buoyant fluid particles into the flow, lighting them strongly from the side against a dark background and taking time exposures of their tracks, usually with an exposure

of $\frac{1}{2}$ sec. A photograph showing several of these tracks is shown in plate 3, figure 13, and all the desired quantities can be measured from such photographs. The position of the particle in the vortex comes from the diameter of the helix (corrected for refraction) and the vertical and tangential velocities respectively from the length and number of turns, and the known time interval. Occasionally, particles were photographed during the time their vertical velocity was changing sign, and a direct measurement could thus be made of the position where this occurred, and the corresponding radial velocity. We shall concentrate on two

Expt. no.	Rate of bubbling (cc/min)	Upper boundary	Rotation rate (rad/sec)	r_0 (cm)
B	400	Free	3π	0·64
I	400	Rigid	3π	0·58
II	1000	Rigid	3π	0·64
V	400	Rigid	2π	0·75
VI	1000	Rigid	2π	0·61

TABLE 2. Experimental conditions for the five runs which are to be compared with the theory

sets of experimental conditions for which most of the relevant quantities were measured, but some data will be presented from all the experiments described in table 2. Not all of the measurements in each experiment were made at the same time, but they were all under nominally the same conditions of bubbling and the rotation rates. In all these cases the depth of the water was 30 cm and the tube through which air was bubbled was placed 10 cm below the surface. Some parts of the experiments were conducted in a 15 cm diameter and some in a 22 cm diameter cylinder, but no difference between these was detected. The geometry of the vortex seems to be governed entirely by that of the region of convection above it, and not at all by the presence of a container at a distance of 3 or 4 times the radius of the region of vertical motion.

Vertical velocity measurements

Profiles of vertical velocity can be measured easily only with a free surface, since otherwise averaging over too many particles is required. These profiles are not very precise because of the vertical oscillations still present and the small velocities produced by residual buoyancies of the tracer particles. In figure 14 are shown vertical velocities as a function of radius for experiment B measured over a small range of depths near the middle of the vortex. They are compared with the form (10) introduced in § 3: the horizontal scale is fixed by the measured position of zero w, and the vertical scale has been adjusted to give the best fit. The agreement is fairly good, but it is clearly impossible with this limited accuracy to provide a critical test of the form of the vertical profile. In particular, there were no particles near the centre in this experiment and the shape in this region has not yet been examined properly.

Photographic measurements of this kind are certainly not good enough to define the rate of variation of w with height. This could only be measured with

adequate accuracy in a few subsidiary experiments, by averaging over a large number of particles injected directly up the centre of the vortex from a hole in the bottom of the tank. These particles (about 30 for each point) were timed over a series of height intervals using a stop-watch, and the results for experiments V and VI are shown in figure 15. They are well fitted by straight lines, thus confirming the result (7) imposed by the conditions for a strong vortex, and permitting the direct determination of $w(0, 0)$ and l. These values, and the quantities

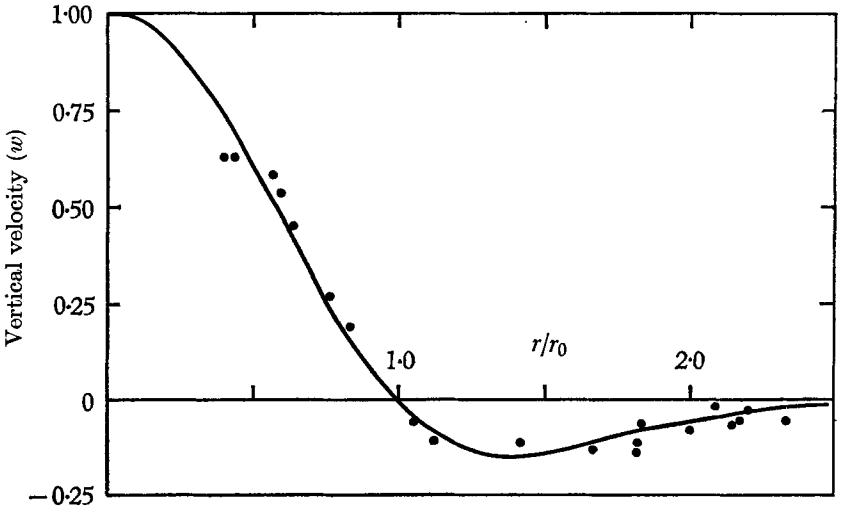

FIGURE 14. Relative measurements of vertical velocity compared with the form (10) (adjusted in both directions to give the best fit). The form of vertical velocity near the axis has not yet been measured.

deduced from them in the manner summarized in § 8, are shown in table 3. It is seen that ϵ is indeed small, and N is close to the value suggested theoretically (certainly within the experimental error). Note that this is so even though all the parameters have varied simultaneously. Comparison of these two experiments illustrates the effect of changing the bubbling rate, with a constant geometry and rate of rotation. Increased 'convection' increases the vertical velocity near the top of the tank (and also the maximum tangential velocity, as we shall discuss later) but it decreases the vertical velocity near the bottom boundary. It also leads to a decrease in r_0, and most important, to a decrease in l, so that the net effect is to increase the radial velocity u_0.

In several other experiments, direct estimates of the maximum radial velocity could be made, and these were typically 0·1 cm/sec, leading to N in the range 10–12. In view of the errors involved in measuring such small velocities, these are not significantly different from the values based on vertical velocity.

Tangential velocity profiles

The tangential velocity profiles derived from the angular velocity measurements in all the experiments described in table 2 will be displayed in two ways. First, in figure 16, they have been plotted directly as tangential velocity against

radius, and then in figure 17 in non-dimensional form using the measured r_0 as the radial length scale and Ωr_0 as the velocity scale. No variations of v with height could be detected in these measurements.

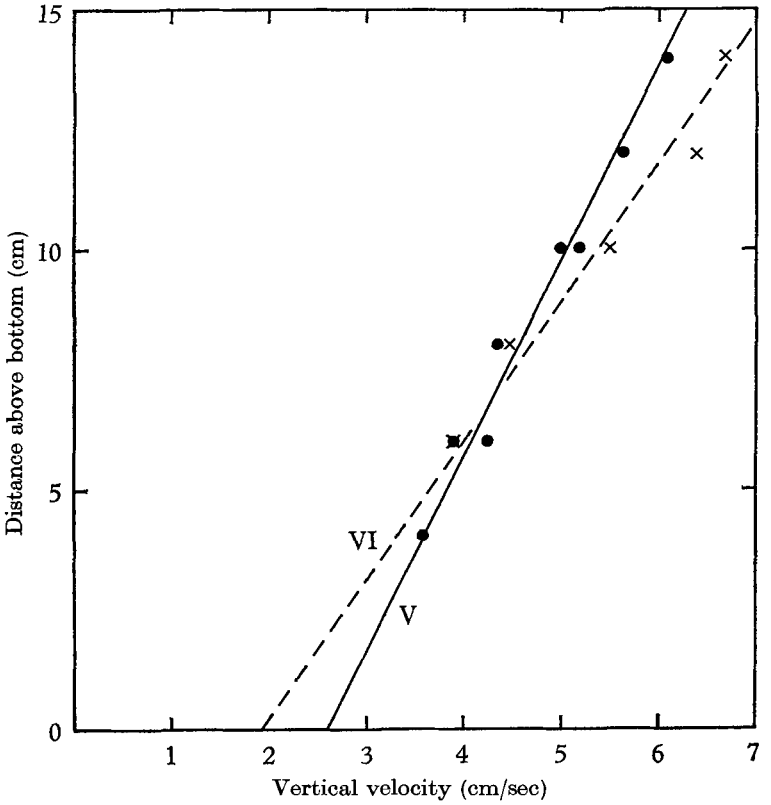

FIGURE 15. Measurements of vertical velocity as a function of height for runs V and VI, obtained by averaging over a large number of neutrally buoyant particles injected up the axis.

Expt. no.	$w(0, 0)$ (cm/sec)	l (cm)	l/r_0	u_0 (cm/sec)	ϵ	N	C
V	2·6	10·6	14	0·09	0·08	7	7·8
VI	1·9	5·5	9	0·11	0·06	7	5·7

TABLE 3. Numerical values of the parameters arising in our theory, deduced from two experiments in which all the relevant measurements were made.

The profiles in figure 16 are all remarkably similar near the origin, and the range of maximum velocities is small. The motion is being maintained, of course, by a bubbling region which is always nearly the same size and shape, and r_0 varies only within the range 0·58–0·75 cm, but the upper boundary condition and the rate of basic rotation have been varied. The main differences appear in the outer parts of the profiles, and the highest maxima are associated with tangential velocities which remain well above solid rotation to larger radii. This is made even clearer by the non-dimensional plot in figure 17.

In all these profiles, the velocity maximum lies in the range $0{\cdot}5$–$0{\cdot}7r_0$. For the experiments conducted at the higher rotation rate, the central angular velocity and the magnitude of the tangential velocity maximum are consistent with those predicted theoretically using vertical profiles with β about $\frac{1}{6}$ (see

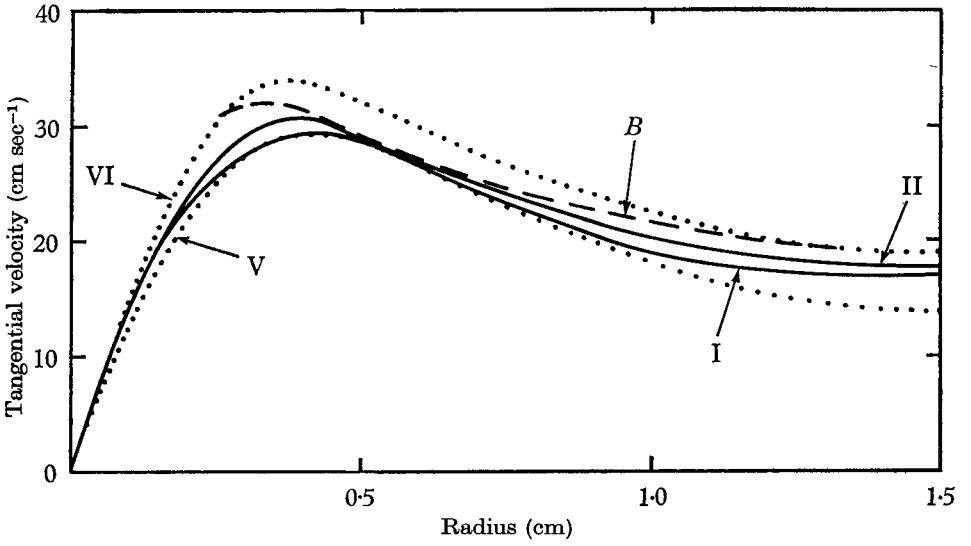

FIGURE 16. Profiles of tangential velocity, deduced from the directly measured angular velocities as a function of radius for the experiments described in table 2.

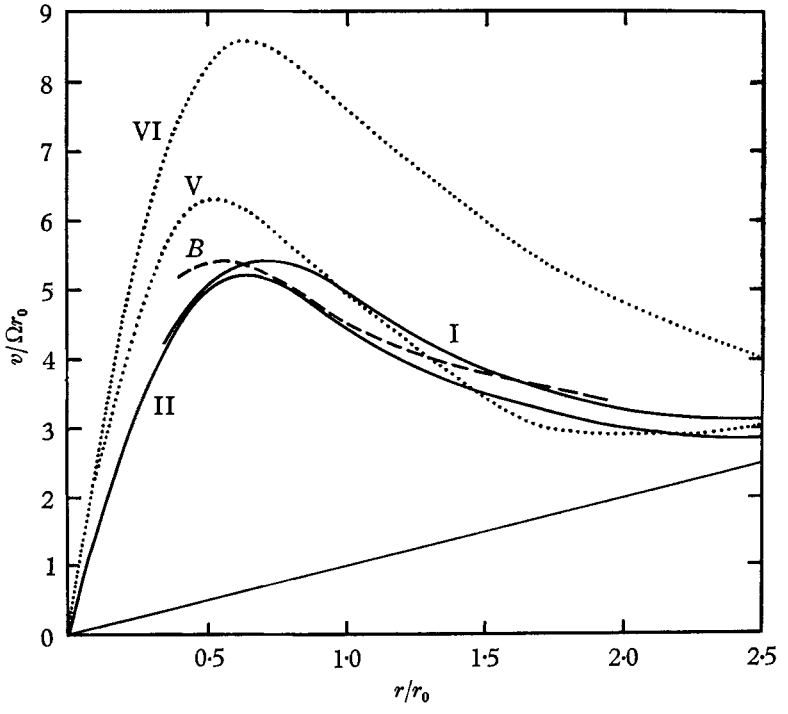

FIGURE 17. The measured tangential velocity profiles of figure 16, made non-dimensional by scaling with r_0 and Ωr_0.

figure 11), and the value of C found in experiment VI is also in accord with this. The main result of using the lower rate of rotation seems to be to allow the region of downward motion to spread sideways to an extent which depends on the rate of bubbling, and thus draw on angular momentum from further off the axis. Experiment V is outside the range covered by the theoretical results, but the increase in magnitude of the maximum and in the value of C are consistent with a return to solid rotation at a larger r/r_0, i.e. an even smaller value of β.

10. Conclusions

The theoretical ideas developed here, which are strongly supported by the qualitative behaviour of our laboratory vortices, and to a lesser extent by the available quantitative results, have led to the following picture of a laminar vortex normal to a rotating solid plane.

With 'strong swirl', in the sense defined above, the tangential and radial velocities are independent of height, and the vertical velocity varies linearly with height. The detailed structure of such a vortex is controlled by the nature of the boundary conditions imposed at the top and bottom. The important quantities which are determined by a region of 'convection' at the top are the radial length scale r_0 and also the ratio $\beta^{\frac{1}{2}}$ of the radii of the upflow (r_0) and a compensating annular downflow. Once the *form* of the vertical flow at the top has been specified, the existence of the bottom boundary imposes a relation between the tangential motion and the vertical velocity just outside the bottom boundary layer. The radial Reynolds number N and the *position* of the tangential velocity maximum $v_{\max}$ relative to r_0 are very insensitive to the upper boundary condition (i.e. to β), while the *magnitude* of $v_{\max}$ and the vertical velocity are calculable, but do depend more strongly on β.

A second geometrical parameter, r_0/l, is left free in this theory. This is a ratio of horizontal to vertical length scales, the latter (l) being defined as the height over which the vertical velocity doubles from its value just above the bottom boundary layer. Thus although the vertical velocity near the bottom is fixed by the geometry of the driving region and the strength of the basic rotation, the magnitude of w higher up can depend separately on the vigour of the convection.

There are of course many gaps in the arguments used, and the arbitrary nature of the imposed stream function is the least satisfactory feature of this analysis. A thorough understanding of the nature of the upper boundary condition, how it controls the horizontal extent of the vertical motion, and how it can impose a vertical velocity distribution which apparently remains nearly similar with height, must certainly be obtained before the problem can be solved completely. The extent to which our assumptions hold in the region beyond the tangential velocity maximum is also worthy of further study. The introduction of higher order terms should not change the structure near the centre, however, and since the local similarity argument is also at its best there, it would be surprising if any major changes could be produced in this way. A more detailed comparison of theory with experiments covering a wider range of parameters would clearly be useful in settling this point.

Though these experiments and the associated theory have emphasized the

importance of the lower boundary to the proper understanding of a vortex above it, their direct relevance to tornadoes is still debatable; the boundary conditions, though more realistic than in some previous models, are still not exactly right. Our recent experimental effort has been concentrated on the problems of maintaining a steady vortex over a *fixed* plane, and of finding a method of driving from above which can impose a measure of external control on the vortex, while still retaining the self-regulating property of the flows driven by convection. It would also be desirable to produce a vortex in which the circulation tends to a constant value at a large radius, rather than having solid rotation there. A separate point, taken for granted in discussing most models but deserving further thought, is the question of the usefulness of laminar models in general. The application of laboratory vortex models to the atmosphere has usually involved replacing molecular viscosity by a constant eddy viscosity determined by the state of the environment, but it seems more likely that the turbulence in the tornado is self-regulating, much as it is in a non-rotating turbulent jet.

This is Contribution no. 1738 from the Woods Hole Oceanographic Institution, and has been supported in part by N.S.F. Grant no. GP 317 and ONR Contract no. 2196. I am grateful to my colleagues at Woods Hole, and to the many visitors, too numerous to mention individually, who have made helpful comments about my experiments and have criticized earlier versions of this manuscript. Mrs Jacqueline Webster was of great assistance in programming some of the calculations for machine computation.

REFERENCES

BATCHELOR, G. K. 1951 *Quart. J. Mech. Appl. Math.* **4**, 29.

BÖDEWADT, U. T. 1940 *Z. angew. Math. Mech.* **20**, 241.

DONALDSON, C. DU P. & SULLIVAN, R. D. 1960 *Proc. Heat Transfer and Fluid Mech. Inst., Stanford University*, no. 16.

EINSTEIN, H. A. & LI, H. L. 1951 *Proc. Heat Transfer and Fluid Mech. Inst., Stanford University*, no. 33.

FULTZ, D. 1951 *Compendium of Meteorology*, p. 1235. Amer. Met. Soc.

GUTMAN, L. N. 1957 *Izv. Akad. Nauk. SSSR (geofiz. ser.)*, **1**, 79.

VON KÁRMÁN, T. 1921 *Z. angew. Math. Mech.* **1**, 244.

KÜCHEMANN, D. 1965 *J. Fluid Mech.* **21**, 1.

LEWELLEN, W. S. 1962 *J. Fluid Mech.* **14**, 420.

LONG, R. R. 1958 *J. Met.* **15**, 108.

LONG, R. R. 1961 *J. Fluid Mech.* **11**, 611.

MACK, L. M. 1962 *Jet Propulsion Lab. Tech. Rep.* no. 32-224.

ROGERS, M. H & LANCE, G. N. 1960 *J. Fluid Mech.* **7**, 617.

ROSENZWEIG, M. L., LEWELLEN, W. S. & ROSS, D. H. 1964 *AIAA J.* **2**, 2127.

ROTT, N. 1958 *Z. Angew. Math. Phys.* **9B**, 543.

ROTT, N. & LEWELLEN, W. S. 1964 *Aerospace Corp. Rep.* No. ATN-64(9227)-6.

ROTT, N. & LEWELLEN, W. S. 1965 *AGARDograph* 97, '*Recent Developments in Boundary Layer Research*', p. 613.

THORARINSSON, S. & VONNEGUT, B. 1964 *Bull. Amer. Met. Soc.* **45**, 440.

TURNER, J. S. & LILLY, D. K. 1963 *J. Atmos. Sci.* **20**, 468.

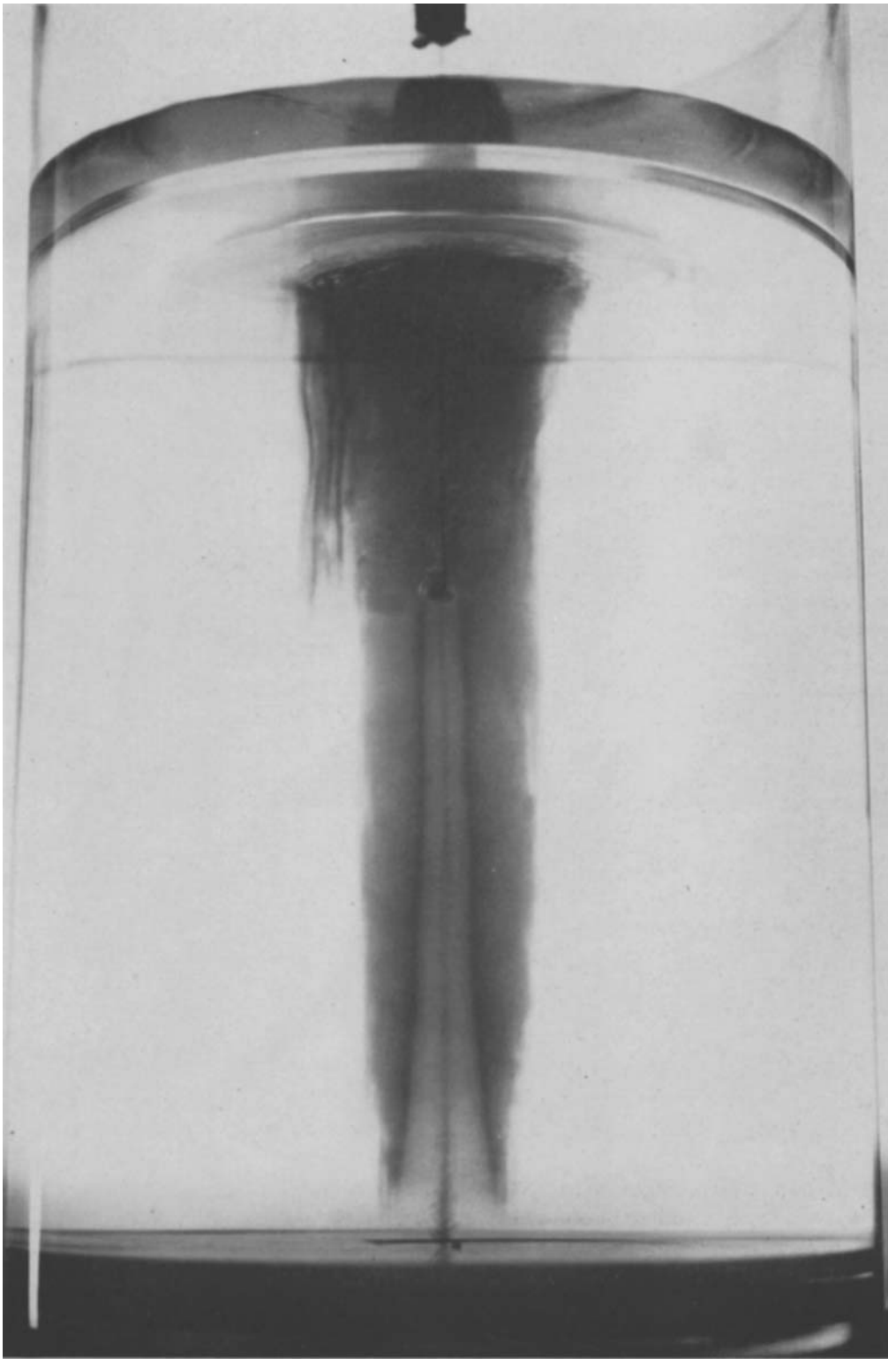

FIGURE 1. Photograph of a vortex driven from above by convection produced by a stream of air bubbles. A dye crystal on the bottom shows the upward motion in the centre, and dye put in at the top marks an annular downflow.

TURNER

(*Facing p.* 400)

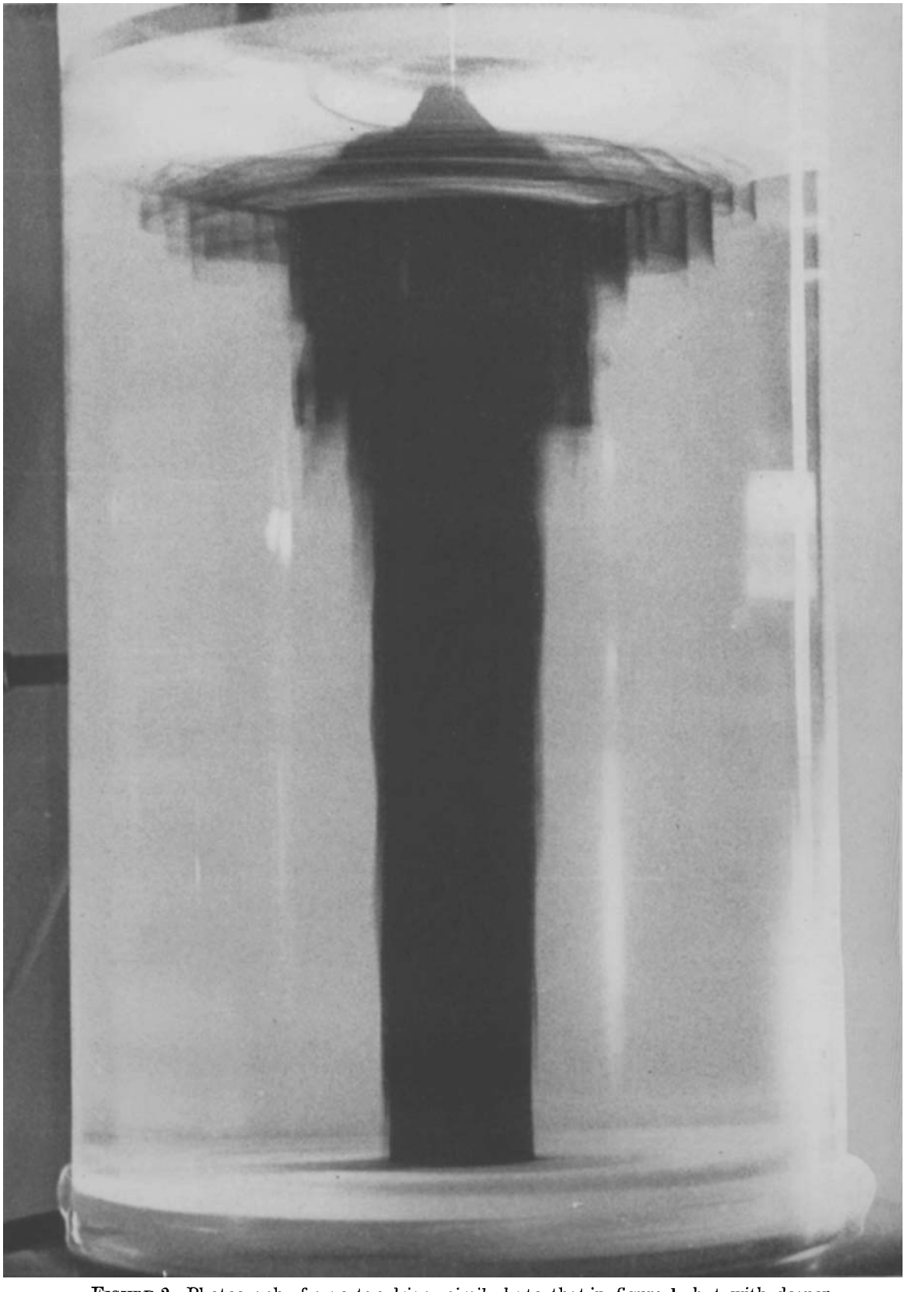

FIGURE 2. Photograph of a vortex driven similarly to that in figure 1, but with deeper dye put in at the top and left for a longer time. The dye, and the downward motion, is confined to a cylindrical region round the axis; on reaching the bottom, fluid flows rapidly inwards in a thin boundary layer and up the centre.

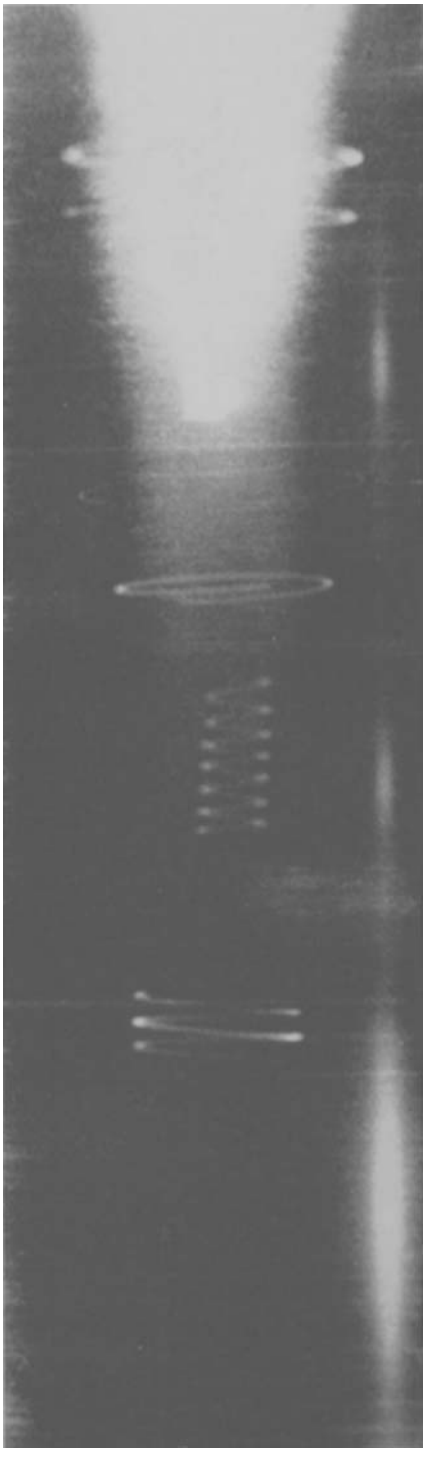

FIGURE 13. The method of velocity measurement. Time exposures of illuminated neutrally buoyant particles give spiral tracks whose dimensions are a measure of position and the three velocity components. This is an enlarged view of the central part of the tank just below the air bubbles.

TURNER